# Sialoglycans Modulate Siglec-5 – TLR4 Interactions in Osteoarthritis

**Authors:** Loise Råberg[1], Fan Jia[1], Ula von Mentzer[1], Vignesh Venkatakrishnan[1], Niclas G. Karlsson[2], Alexandra Stubelius[1*]

**Affiliations:**

[1] Division of Chemical Biology, Department of Life Sciences, Chalmers University of Technology, Gothenburg, SE-412 96, Sweden.

[2] Department of Life Sciences and Health, Faculty of Health Sciences, Oslo Metropolitan University Oslo Metropolitan University, Oslo, Norway

[*]**Corresponding author:**

Alexandra Stubelius (alexandra.stubelius@chalmers.se)

Chalmers University of Technology

Department of Life Sciences

Division of Chemical Biology

Kemigården 4

SE-412 96 Göteborg,

Sweden

+46(0)31-772 4101

**Keywords**: Osteoarthritis, Monocytes, Siglec-5, Sialic Acid, TLR4

**Summary:**
Osteoarthritis (OA) is characterized by chronic, low-grade inflammation that contributes to cartilage degradation and joint pain. We previously identified Siglec-5/14 in synovial fluid of OA patients (OA SF), which prompted us to investigate its interaction with the sialylated proinflammatory receptor TLR4 in monocytes. Here, we reveal an inverse correlation between Siglec-5 and TLR4, suggesting Siglec-5 may suppress inflammation. To gain mechanistic insights, monocytes stimulated with OA SFs were compared to M-CSF, LPS, and sialidase, to assess patient-specific inflammatory pathways and phenotypes. Notably, OA SF that triggered elevated IL-6 production in monocytes exhibited phenotypes similar to those of LPS- or sialidase-treated cells, reinforcing the role of sialylation patterns influencing OA severity. To confirm direct interaction of Siglec-5 and TLR4, colocalization was analyzed, displaying a time- and sialoglycan- dependent interaction. These findings reveal a Siglec-5-TLR4 axis modulated by sialylation, highlighting a potential strategy for mitigating inflammation and preserve joint integrity in OA.

# INTRODUCTION

Osteoarthritis (OA) is the most common degenerative joint disorder worldwide, characterized by synovitis, cartilage degradation and subchondral bone remodeling that severely impacts quality of life. [1] This complex condition involving mechanical stress and inflammatory pathways displays significant variability between patients. Persistent inflammation stem from both tissue-resident and infiltrating immune cells, including monocytes, which play key roles in perpetuating inflammation. [2,3] Upon recruitment, monocytes are polarized into a pro-inflammatory phenotype in response to the local environment, contributing to the cycle of tissue damage and degeneration of cartilage. [4,5] The multifactorial nature of OA coupled to the limited regenerative capacity of cartilage has posed a major challenge both for finding relevant biomarkers and developing effective treatments. Despite extensive efforts, clinical trials targeting cytokines such as IL1β and TNFα have not yielded significant therapeutic benefits, underscoring the need for alternative mechanistic insights and novel intervention strategies. [6-8]

Recent advances in nanotherapeutics have offered promising new approaches, as they can deliver drugs to the deeply embedded cells in the cartilage responsible for OA progression. [9] In our previous work, we explored the interactions between a family of small dendritic polyamidoamine (PAMAM)-based nanoparticles (NPs) and synovial fluid (SF) proteins from OA patients. [10] By proteomics, we identified a high abundance of Sialic acid-binding immunoglobulin-like lectin-5/14 (Siglec-5/14) in the proteins associated with the NPs, suggesting a potential involvement in OA pathogenesis. Despite their opposing immunological roles, Siglec-5 and Siglec-14 share a high degree of extracellular sequence homology, which makes them difficult to distinguish experimentally. [11] Siglecs are gaining increasing attention in multiple diseases, including cancer, sepsis, and autoimmune disorders due to their immunomodulatory functions and potential for therapeutic targeting. [12-14] Siglec-5 has been found in sepsis, Siglec-9 in arthritis, and Siglec-15 plays an important role in macrophage fusion into osteoclasts but so far, the role of Siglec-5 and Siglec-14 has not been reported in OA. [15-17] Through their affinity to sialic acid (Sia), inactivating Siglecs such as Siglec-5 act as key regulators of monocyte activation, recruiting the tyrosine SHP-1 and SHP-2, to counterbalance pro-inflammatory pathways, [18] whereas activating Siglecs, like Siglec-14 signal through DAP12. [11] Siglec-5 is mostly found on cell surfaces on monocytes, macrophages, and T cells. However, soluble Siglec-5 has been identified and was shown to inhibit $CD8^+$ T cell proliferation in sepsis, and soluble Siglec-9 demonstrated immunosuppressive effects on macrophages in arthritis models. [15,17,19] The generation of soluble Siglec-14 has been well characterized, where one study demonstrated that it can inhibit the interaction between membrane-bound Siglec-14 and TLR2. [20]

In arthritis, upregulated Siglec-9 has been identified and murine Siglec-E, the mouse ortholog of human Siglec-9 has been shown to regulate pattern recognition receptors (PRRs). [15,21] PRRs, such as toll-like receptor 4 (TLR4), play a key role in OA, its activation can be induced by structural fragments of damaged cartilage. [22,23] TLR4 recognizes solubilized fragments of glycoproteins such as collagen type-II, hyaluronan, aggrecan, and lubricin which are present in OA SF and function as damage-associated molecular patterns (DAMPs), thereby

exacerbating joint inflammation. [24-26] TLR4 is gaining increasing interest as its activation disrupts immune homeostasis and contributes to the onset and progression of age-related diseases, including OA. [27] Through the NF-κB pathway pro-inflammatory cytokines such as IL-1, IL-6, IL-8, and tumor necrosis factor (TNFα) are released in the joint, aggravating joint degradation and OA symptoms, however its regulation is poorly understood in OA. [3,23,28-31] TLR4 activity is influenced by its internalization dynamics and glycosylation decorations. Specifically, its sialylation patterns play a pivotal role in modulating TLR4 signaling. [21,32,33] In general, endogenous activity of sialyltransferases and sialidases are regulated upon monocyte activation and differentiation, and alteration in sialyltransferase expression have been identified in OA cartilage. [34-36] It has been shown that LPS can trigger sialidase relocation to the cell surface, where it desialylates TLR4 and promotes its activation. [37] Interestingly, Siglec-E counteracts this process by binding Sia residues on TLR4, leading to either internalization or shedding of TLR4 to reduce inflammation. [21,38-40] Both Siglec-9 and Siglec-5 have shown high affinity to TLR4, indicating their immunomodulatory role of TLR4 signaling.[32] Siglec-5 has however not been studied as extensively as Siglec-9, which could be due to lack of a mouse ortholog. [17,18] As we had identified Siglec-5/14 in the SF of OA patients, the purpose of this study was to investigate the regulatory relationship between Siglec-5, Siglec-9, Siglec-14, Siglec-15 and TLR4 in monocyte stimulated with OA SF.

We found an inverse correlation between membrane-associated Siglec-5/14 and TLR4 expression by flow cytometric profiling, suggesting that engaging Siglec-5/14 dampens excessive inflammatory responses. To gain mechanistic understanding we employed stimulations including macrophage-colony stimulating factor (M-CSF), IL1β/TNFα, LPS, and sialidase to understand patient-specific inflammatory pathways and phenotypes. Further insights of crosstalk between Siglec-5 with TLR4 and Siglec-9, was gained through inhibition of TLR4 signaling using the small molecule inhibitor TAK-242. Our findings suggest that Siglec-5 can serve as a modulator of TLR4-driven low-grade inflammation. High-grade inflammatory conditions induced by LPS or sialidase displayed similar cytokine profiles both with and without TAK-242, indicating that sialoglycans are critical regulators of TLR4-driven inflammation. Overall, our findings suggest that Siglec-5, but not Siglec-9, Siglec-14 and Siglec-15, through Sia expression on cells could present an endogenous regulatory pathway to fine tune and mitigate inflammation to reduce cartilage degradation in OA.

# RESULTS

**Siglec-5/14 can be found in synovial fluid from osteoarthritis patients and membrane-associated Siglec-5/14 negatively correlates with TLR4 expression on monocytes**

NPs can be used as enrichment tools to identify proteins associated with pathogenic regulation. In a previous study, we developed a set of NPs which were incubated with OA SF where the proteins were identified through proteomics.[10] Amongst the proteins found in association with the NPs we identified Siglec-5/14 as one of the 14 most abundant entities (Figure 1A). As Siglec-5 functions as an inhibitory receptor, we used the IntAct database to

find a potential regulated partner and discovered a medium relationship (MI score 0.54) between TLR4 and Siglec-5, but not Siglec-14 (Figure 1B), suggesting an unexplored regulatory pathway in OA.[41] Interestingly, both of these receptors can be found on monocytes, which is the most abundant immune cells in the OA joint .[42]

Monocyte function can be classified into different subsets based on their expression of CD14 and CD16.[43,44] The intermediate $CD14^{+}CD16^{+}$ subset presents antigens and secretes cytokines and has been found in greater abundance in the joint of OA patients.[42] In this study, we isolated blood-derived monocytes and confirmed their relative percentage of subsets (Figure S1, Figure S2A and S2B). Figure 1C shows the gating strategy at baseline, where all monocytes were positive for Siglec-$5^{+}$ (purple) and Siglec-9 (not shown), whereas the percentage $TLR4^{+}$ monocytes were mainly found in the classical and intermediate population (green). We found that monocytes cocultured with OA SFs for 24hrs generated an intermediate monocyte population consisting of more than 50% of the population (Figure 1D and 1E). Compared to baseline, the classical monocytes decreased, and non-classical monocytes were completely absent. While most cells remained positive for Siglec-5 (purple), TLR4 (green) expression was reduced.

The monocyte subsets were further analyzed for their baseline expression of TLR4, Siglec-5/14, Siglec-9, and Siglec-15. Classical monocytes displayed the highest expression of TLR4, Siglec-5/14, and Siglec-9, whereas Siglec-15 was not detected on any subset (Figure S2C-E and Figure S3). After 24h of OA SF stimulations, multiple OA SFs led to a significant upregulation in Siglec-5 expression on monocytes (Figure 1G). In contrast to previous murine studies, Siglec-9 was only upregulated in one patient (Figure 1H). Correlation analysis confirmed an inverse relationship between Siglec-5/14 with TLR4 and intermediate monocytes (Figure 1I and 1J), whereas no correlation was observed between Siglec-9 with TLR4 and intermediate monocytes (Figure 1K and 1L). A correlation between Siglec-5/14 to Siglec-9, and intermediate monocytes to TLR4 could not be established (Figure S4A and S4B).

In summary, the monocytes shifted toward the intermediate subset after SF stimulation. Correlation analysis revealed an inverse relationship between Siglec-5/14, TLR4, and intermediate monocytes, but not with Siglec-9, suggesting interactions specifically between TLR4 and Siglec-5 in OA.

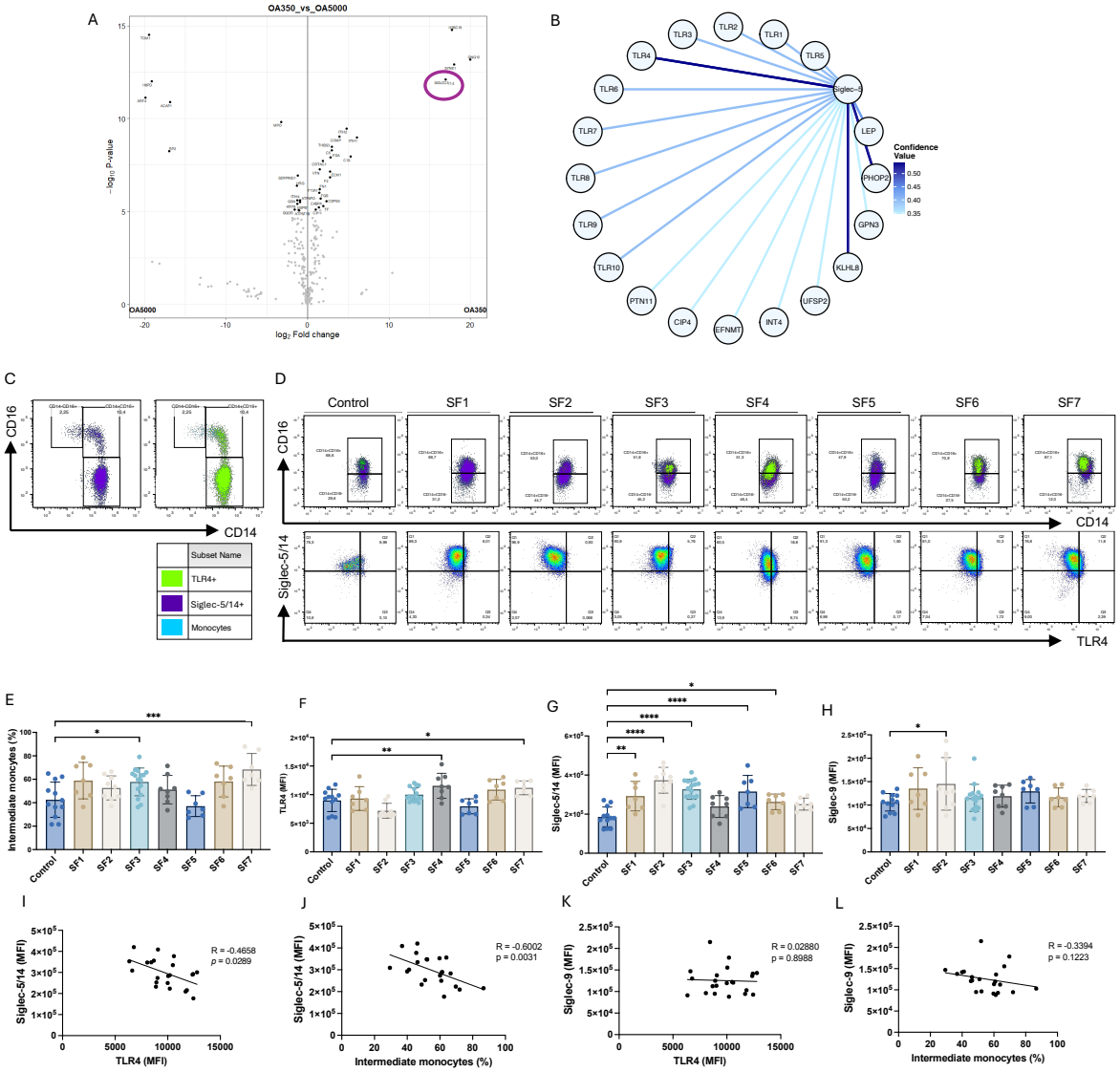


**Figure 1. Siglec-5/14 can be found in synovial fluid from osteoarthritis patients and membrane-associated Siglec-5/14 negatively correlates with TLR4 expression on monocytes**

(A) Volcano plot displaying the proteins detected in the protein in association with $PAMAM_{5000}$ and $PAMAM_{350}$, here denoted OA5000 and OA350 using proteomics analysis. Siglec-5/14 is indicated with a circle.

(B) Protein-protein interaction network visualized from the IntAct database. Medium evidence of interaction appears to TLR4, PHOP2, and KLHL8, where TLR4 had the highest confidence value with a MI score of 0.54. The illustration was adopted from the website and resolution and color scheme improved using R.

(C) Representative flow cytometric dot plots displaying the baseline levels (0hrs) of classical, intermediate, and non-classical subsets, where blue color represents all monocytes, purple color represents Siglec-5/14$^{+}$, and green represents TLR4$^{+}$ cells.

(D) Representative flow cytometric dot plots of monocytes after 24hrs of coculture with OA SF. The plots display the ratio between classical and intermediate monocytes, where blue represents both subsets, purple represents Siglec-5/14$^{+}$ cells, and green represents TLR4$^{+}$ cells.

(E) Percentage intermediate monocytes ($CD14^+CD16^+$) after 24hrs of coculture with OA SF. Each datapoint represents one technical replicate from three independent biological replicates.

(F-H) Median fluorescence intensity (MFI) of TLR4, Siglec-5/14, and Siglec-9 on the cell membrane of monocytes after 24hrs of coculture with OA SF. Each datapoint represents one technical replicate from three independent biological replicates.

(I-L) Correlation between Siglec-5/14 to TLR4 and intermediate monocytes, and between Siglec-9 to TLR4 and intermediate monocytes. Each datapoint is the mean from three technical replicates from three donors exposed to SF1-7, except SF3 which was evaluated on four different donors.

Data is represented as mean±SD, statistical analysis was performed using one-way ANOVA with Dunnett's multiple comparisons test. Correlation analysis was performed using Spearman's correlation test (*$p$<0.05; **$p$<0.01; ***$p$<0.001; ****$p$<0.0001).

**Siglec-5 regulate TLR4 signaling in inflammation**

To investigate how specific signaling pathways dictate membrane expression of TLR4, Siglec-5/14, and Siglec-9, blood monocytes were isolated and subsequently stimulated with either M-CSF, IL1β/TNFα, or LPS. After 24hrs of stimulation with M-CSF and LPS, an expansion of intermediate monocytes where noted compared to baseline levels. The total monocyte population remained Siglec-5/$14^+$, while $TLR4^+$ monocytes decreased in the control and LPS (Figure 2A). We further assessed the expression dynamics of TLR4, Siglec-5/14, and Siglec-9 levels at 0, 4 and 24hrs of stimulation (Figure 2B-D). An initial increase in TLR4 could be observed already after 4hrs in the control and M-CSF, which remained after 24hrs. LPS reduced TLR4 expression already within 4 hours and this effect remained after 24hrs. Siglec-5/14 decreased across all groups after 4hrs of stimulation but recovered to basal level expression by M-CSF and LPS stimulations after 24hrs. All stimulations induced Siglec-9 expression after 4 and 24hrs compared to basal levels.

We proceeded with comparing the dynamics of the expression of intermediate monocytes, TLR4, Siglec-5/14, and Siglec-9 at 4 and 24hrs. For most stimulations, intermediate monocytes expanded continuously over 24hrs (Figure S5A, Figure 2E). TLR4 expression increased initially by M-CSF, while LPS reduced the expression of TLR4 compared to control at 4hrs (Figure S5B). After 24hrs, LPS continued to reduce TLR4 expression, whereas M-CSF and IL1β/TNFα produced comparable levels to control (Figure 2F, Figure S6A). Compared to the control, Siglec-5/14 and Siglec-9 expression remained the same across all stimulations at 4hrs (Figure S5C and S5D). After 24hrs of stimulation, M-CSF, IL1β/TNFα, and LPS had all induced a significant increase in Siglec-5/14 (Figure 2G, Figure S6B). In contrast, no significant alterations in Siglec-9 expression were observed by any stimulations at 24hrs (Figure 2H). To assess whether the shifts were due to Siglec-5 or Siglec-14, a Siglec-14 specific antibody was used. We found no significant change in membrane expression of Siglec-14 between the control, M-CSF, and LPS (Figure 2I). Siglec-5 mediates its inhibitory immune regulation by recruiting SHP-1 and SHP-2. To confirm that the mechanism involved Siglec-5 rather than Siglec-14, the SHP-1 inhibitor TPI-1 (100ng/mL) was added one hour

prior to adding M-CSF and LPS. After 4hrs, supernatants were collected and analyzed for cytokine production using the LEGENDplex assay. LPS-stimulated monocytes produced higher levels of IL1β, IL-10, and IL-23 compared to those treated with TPI-1. In contrast, inhibition of SHP-1 resulted in increased production of MCP-1, IL-6, IL-8, and IL-18 by LPS-stimulated monocytes.

In summary, the intermediate monocyte population expanded over time, where TLR4 was reduced as Siglec-5 increased, displaying an interesting dynamic regulation pattern. This was true for both M-CSF and LPS, whereas IL1β/TNFα showed little regulation. Our data suggests complex interacting mechanisms governing TLR4 signaling, ultimately shaping the monocyte response in OA.

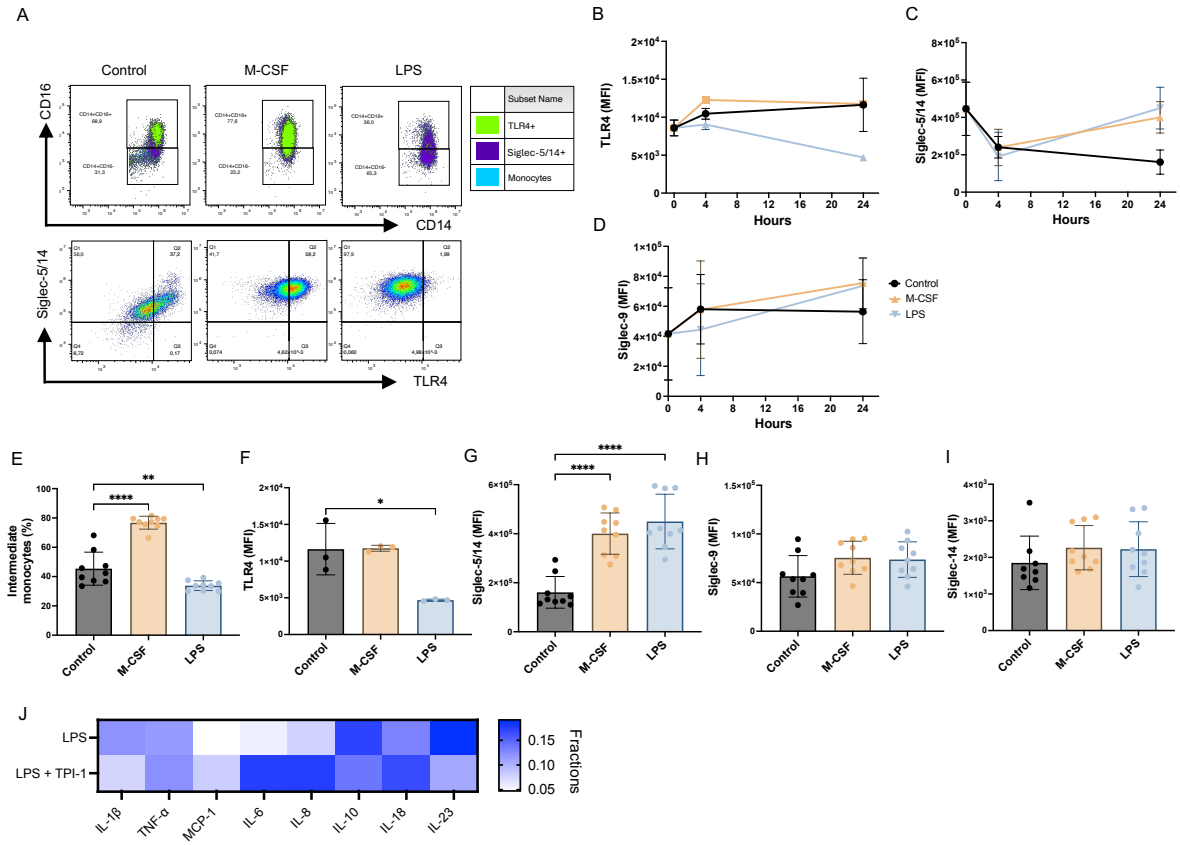


**Figure 2. Siglec-5 regulate TLR4 signaling in inflammation**

(A) Representative flow cytometric dot plots displaying the percentage classical and intermediate monocytes in the control, and M-CSF- and LPS-stimulated monocytes. Blue represents all cells, green represents TLR4$^{+}$ cells, and purple represents Siglec-5/14$^{+}$ cells, which can also be displayed in the row of dot plots below.

(B-D) MFI of membrane-associated TLR4, Siglec-5/14, and Siglec-9 was assessed at 0, 4, and 24hrs of stimulation with M-CSF and LPS and compared to the control.

(E) The percentage intermediate monocytes after 24hrs in the control, and monocytes stimulated with M-CSF and LPS.

(F-I) MFI of membrane-associated TLR4, Siglec-5/14, Siglec-9, and Siglec-14 in the control and monocytes stimulated with M-CSF and LPS for 24hrs.

(J) Cytokines produced by monocytes stimulated with LPS with and without the SHP-1 inhibitor TPI-1 (100ng/mL) was analyzed using the LEGENDplex Human Inflammation Panel 1 (13-plex). Cytokines with levels below the detection limit were excluded from analysis.

Each datapoint represents one technical replicate, with three technical replicates performed for each of three independent biological replicates, except for TLR4 which was measured on one biological replicate. Data is represented as mean±SD, statistical analysis was performed using one-way ANOVA with Dunnett's multiple comparisons test (*$p$<0.05; **$p$<0.01; ***$p$<0.001; ****$p$<0.0001).

**Siglec-5 and TLR4 co-localization on the cell surface of monocytes**

Both Siglec-5 and TLR4 are transmembrane receptors which engages extracellularly at the cell-membrane surface as well as interacts with intracellular ligands to induce intracellular signaling cascades. To understand where the receptors could potentially interact, we performed an in-silico protein-protein prediction in AlphaFold3 for direct contact between TLR4 and Siglec-5 (Figure S7). [45] For both Siglec-5 and TLR4, a per-residue pLDDT plot identified both confident (70+) secondary structures indicated by blue colors, as well as less confident structures (below 70) indicated by yellow and orange colors. Siglec-5's intracellular domain consisted of intrinsically disordered regions (IDR), making predictions increasingly difficult. When analyzing the output data from the modeling, the predicted aligned error (PAE) in the relative position and orientations of the proteins revealed several potential interaction points between the proteins, both the resulting predicted template modeling (pTM) score of 0.47 and ipTM score of 0.21 indicated low confidence and an overall challenging prediction. However, the current limitations of glycan interactions in AlphaFold made it challenging to draw any valuable conclusions as Siglec-5 will bind to Sia.

We therefore used immunocytochemistry to investigate the spatial expression patterns and potential physical interactions on monocytes. Here we used an antibody with affinity to a protein sequence found in Siglec-5 and not Siglec-14. Representative images show localization of TLR4 (green) and Siglec-5 (red) under each condition (Figure 3A). Both Siglec-5 and TLR4 displayed uniform expression at 0hrs, which changed after 24hrs in culture. As with flow cytometry, a decrease was noted in TLR4 by LPS, whereas Siglec-5 maintained a uniform expression pattern on the cell membrane. At 0hrs, Mander's colocalization coefficient (MCC), determined a strong TLR4 overlap with Siglec-5 (MCC = 0.78), while the more abundantly expressed Siglec-5, as expected, displayed a weak overlap to TLR4 (MCC = 0.35; Figure 3B and 3C). After 24hrs of stimulations, all conditions led to a reduction in TLR4 overlap with Siglec-5, with MCC values ranging between 0.46-0.50, indicating a moderate overlap. Cells stimulated with LPS had lost the correlation between Siglec-5 and TLR4 and now showed no evidence of interaction.

In conclusion, the immunocytochemistry data indicated a potential for these receptors to physically interact on the cell membrane and be regulated by M-CSF and LPS.

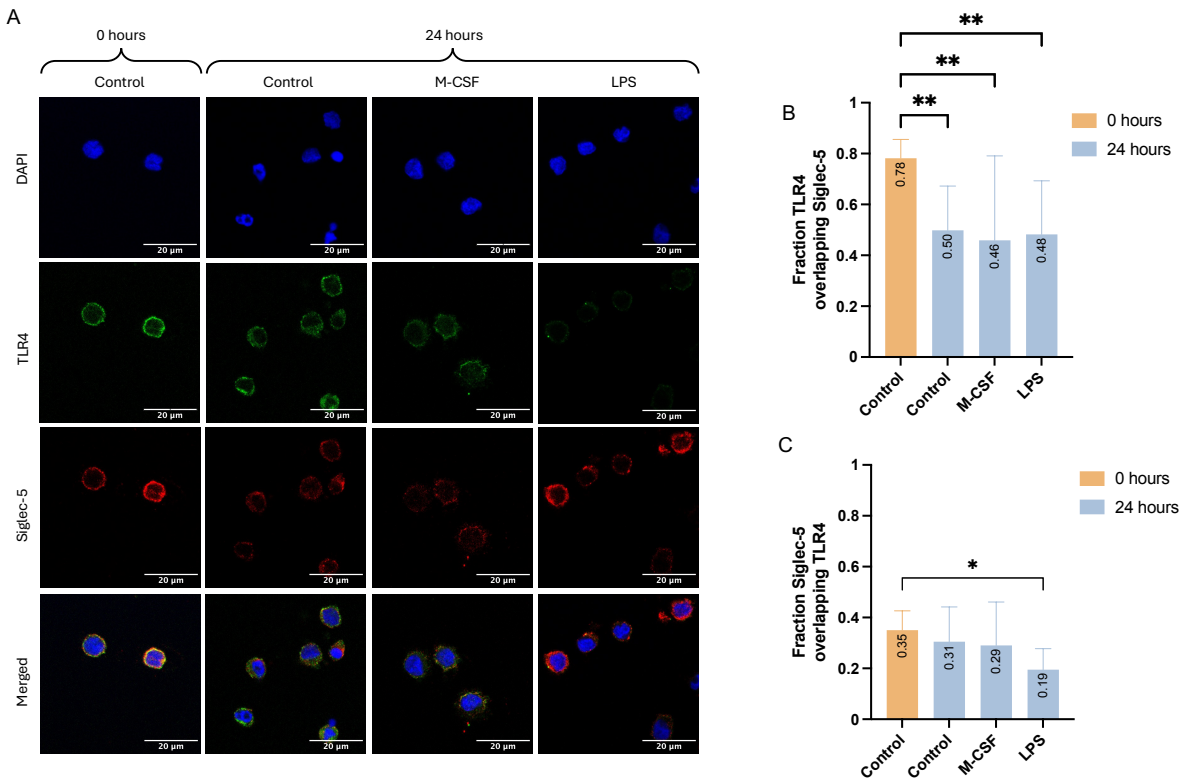


**Figure 3. Siglec-5 and TLR4 co-localization on the cell surface of monocytes**

(A) Representative immunofluorescence images of monocytes at baseline, and control, M-CSF, and LPS after 24hrs. Blue color (dapi) colored the nucleus, green color represents TLR4, and red color represents Siglec-5. Scale bar represents 20µm.

(B-C) Mander's colocalization coefficient (MCC) M1: Fraction TLR4 overlapping Siglec-5, and M2: Siglec-5 overlapping TLR4. Data is represented as mean±SD generated from 4-7 images per condition with two biological replicates. Statistical analysis was performed using one-way ANOVA with Dunnett's multiple comparisons test (*$p$<0.05, **$p$<0.01).

**Intracellular inhibition of TLR4 reduced cytokine secretion and Siglec-5 expression**

To assess the functional consequences of Siglec-5/14 and TLR4 interactions, we measured cytokines produced by the monocytes after the stimulations. To deduce if NFkB signaling was the main signaling pathway involved in the interactions we used the small molecule TLR4 inhibitor TAK-242. This inhibitor specifically binds to Cys747 in the intracellular domain of TLR4, inhibiting both MyD88-dependent and MyD88-independent pathways. [46] The involvement of TLR4-signaling was determined by evaluating how effective TAK-242 was in suppressing cytokine production using the bio-plex cytokine screening method. The inhibition was performed prior to the addition of M-CSF, IL1β/TNFα, and LPS and was maintained throughout the experiment.

LPS lead to the most pronounced increase in pro-inflammatory cytokines at both 4hrs (Figure S8A) and 24hrs (Figure 4A). With elevated levels of TNFα, RANTES, IL1β, IL-1ra, MCP-1, IL-10, and G-CSF detected, aligning with its known role to trigger TLR4-mediated inflammation. M-CSF, in contrast, was associated with lower cytokine secretion consistent

with its role in differentiation of monocytes into macrophages. Prominent inhibition of cytokine secretion by TAK-242 was observed after LPS as well as with M-CSF stimulation after both 4 and 24 hours. IL1β/TNFα induced cytokine secretion as well, however the TAK-242 inhibitor had no influence on the signaling and levels of cytokines produced, as expected (Figure S9).

Next, we evaluated how blocking TLR4 affected monocyte subsets, including the intermediate population, as well as the receptors TLR4, Siglec-5/14, and Siglec-9. After 4hrs of stimulation, no significant changes in expression patterns were observed after TAK-242 treatment (Figure S8B-S8E). However, inhibition of TLR4 signaling induced a significant abundance in intermediate monocytes after 24hrs (Figure 4B). TAK-242 only induced significant TLR4 expression after M-CSF activation (Figure 4C). M-CSF and LPS induced the highest levels of Siglec-5/14 and interestingly, blocking TLR4 significantly reduced Siglec-5/14 expression in these two groups (Figure 4D). In contrast, Siglec-9 expression remained unchanged when TLR4 was blocked (Figure 4E). To determine whether TLR4 blockade affected both Siglec-5 and Siglec-14 similarly, we used the Siglec-14 specific antibody and found no significant change in surface expression (Figure S10). TAK-242 had no impact on the fraction TLR4 overlap with Siglec-5 and vice versa (Figure 4F and 4G). These findings suggest that TLR4 inhibition influence Siglec-5 expression.

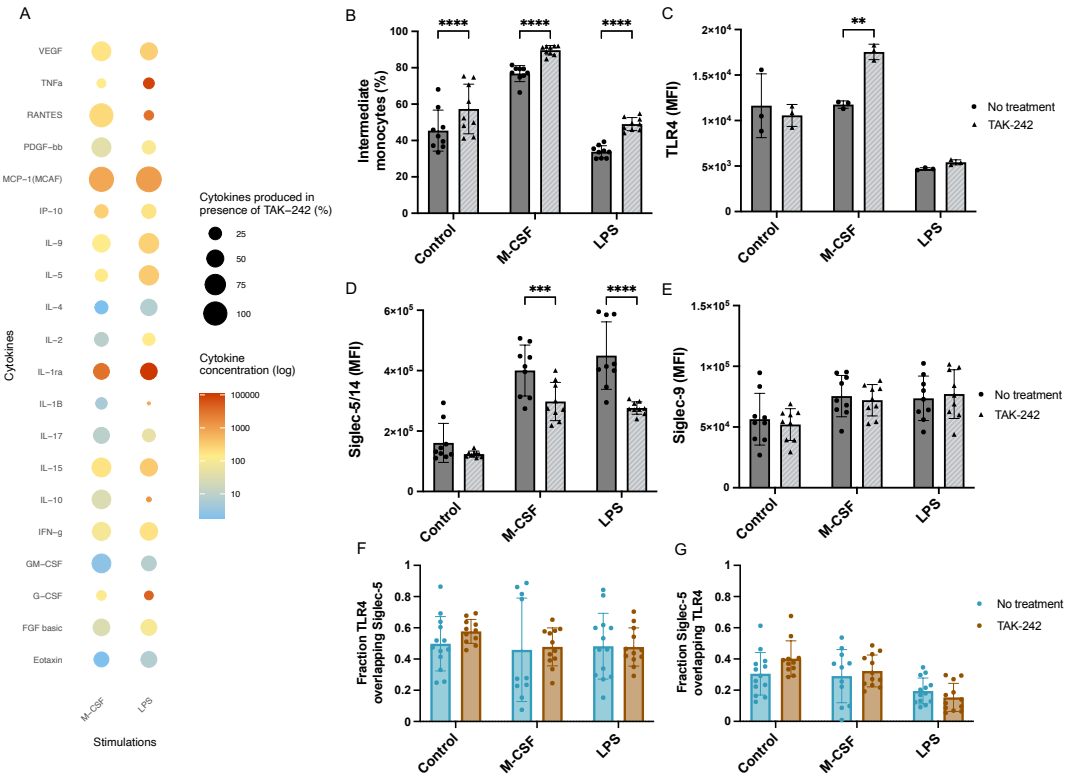


**Figure 4. Intracellular inhibition of TLR4 reduced cytokine secretion and Siglec-5 expression**

**(A)** Using the Bio-Plex Pro Human Cytokine Grp I Panel 27-Plex, a panel of cytokines and chemokines was screened in the supernatants of monocytes incubated for 24hrs with M-CSF and LPS, with and without the TLR4 inhibitor TAK-242. Each datapoint is the mean

of three biological replicates with three technical replicates pooled together. Cytokine levels from monocytes stimulated in absence of TAK-242 is indicated by "Cytokine concentration (log)" and the "Cytokines produced in presence of TAK-242 (%)" indicates how effective TAK-242 was at limiting cytokine secretion compared to without TAK-242.

(B) The percentage of intermediate monocytes after TAK-242 treatment was quantified in monocytes stimulated with M-CSF and LPS and compared to the control at 24hrs. Each datapoint represents one technical replicate. Three technical replicates were used from three biological replicates.

(C-E) The effect of TAK-242 was assessed based on MFI of membrane-associated TLR4, Siglec-5/14, and Siglec-9 in monocytes stimulated with M-CSF and LPS and compared to the control at 24hrs. Each datapoint represents one technical replicate. Three technical replicates were used from three biological replicates, except for TLR4 which was analyzed from one biological replicate.

(F-G) Mander's colocalization coefficient (MCC) displaying fraction TLR4 overlapping Siglec-5 and vice versa. Each datapoint represents one image, 4-7 images were used per condition from two biological replicates.

Data is represented as mean±SD, statistical analysis was performed using two-way ANOVA with Sidak's multiple comparisons test (**p*<0.05; ***p*<0.01; ****p*<0.001; *****p*<0.0001).

**Siglec-5 and TLR4 interaction is abrogated by loss of sialoglycans**

To delineate mechanisms pertaining to Siglec-5 signaling and its correlation to TLR4, sialidase was used to remove membrane-bound Sia and to assess its effect on cell behavior, especially as TLR4 is sialylated. [38] The ability of sialidase to enzymatically remove Sia from glycans was confirmed by LC-MS and lectin staining. An increased level of O-glycans lacking Sia was detected in sialidase treated monocytes (Figure 5A), as well as lower levels of α2,3 and α2,6 Sia in presence of sialidase (Figure 5B and 5C). TLR4 expression was also shown to be reduced after treatment with sialidase, whereas Siglec-5/14 and Siglec-14 displayed similar expression as control (Figure 5D and 5E, Figure S10). The colocalization of TLR4 and Siglec-5 after 24hrs of sialidase treatment was evaluated through immunocytochemistry, which revealed reduced expression of both receptors compared to the control at 0hrs (Figure 5F). The fraction overlap of TLR4 to Siglec-5 (M1), and Siglec-5 to TLR4 (M2) was evaluated using the MCC score (Figure 5G). This revealed a medium TLR4 overlap to Siglec-5 (MCC = 0.47). Similar to LPS, no evidence of overlap between Siglec-5 to TLR4 (MCC = 0.13) was observed. When measuring cytokine production using the bio-plex screening method, treatment with sialidase led to an increase in TNFα, RANTES, IL1β, IL-1ra, MCP-1, IL-10, and G-CSF, the same proinflammatory cytokines as LPS induced (Figure 5H).

Inhibition of TLR4 signaling using TAK-242 in cells treated with sialidase seemed to affect TLR4 surface expression but not Siglec-5/14. Similar to LPS, TAK-242 treatment of cells treated with sialidase was also effective in limiting cytokine secretion, suggesting that

removing extracellular Sia on TLR4 induces both dependent- and independent MyD88 pathways. [46]

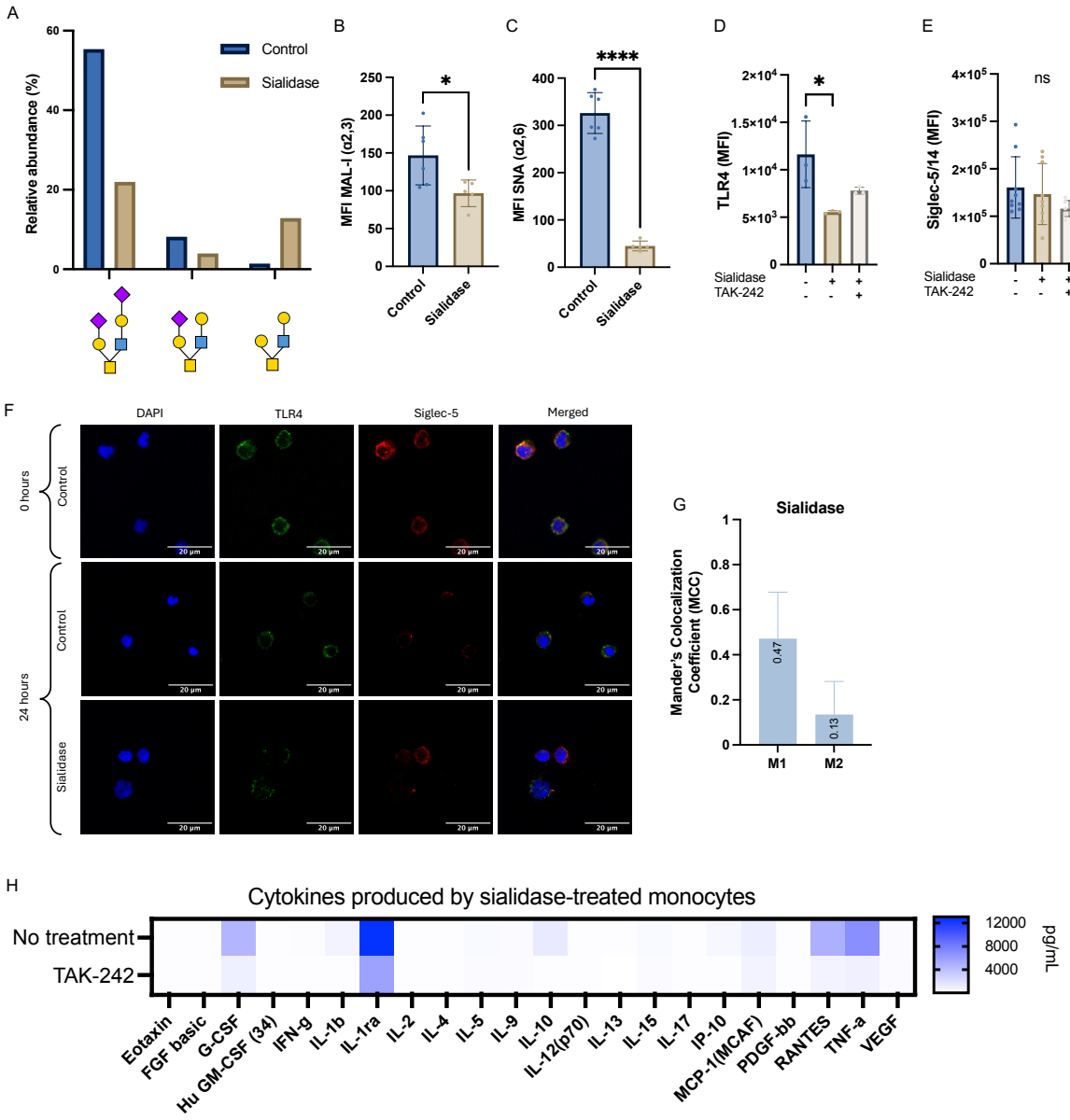


**Figure 5. Siglec-5 and TLR4 interaction is abrogated by loss of sialoglycans**

(A) Sialidase activity was confirmed using LC-MS, the relative abundance of top two sialylated *O*-glycans and non-sialylated *O*-glycan in control and sialidase treated monocytes was quantified.

(B-C) α2,3 and α2,6 Sia on monocytes was quantified in three technical replicates from two biological replicates using MAL-I and SNA lectins. Both linkages significantly decreased in presence of sialidase after 24hrs in culture.

(D-E) Monocytes were enzymatically stripped of their membrane-bound Sia for 24hrs in presence or absence of TAK-242 and compared to the control. MFI of membrane-associated TLR4, Siglec-5/14 and Siglec-14 was assessed in triplicates from one biological replicate for TLR4 and three for Siglec-5/14.

(F) Colocalization of TLR4 and Siglec-5 was investigated in monocytes from two biological replicates treated with sialidase for 24hrs compared to the control at 0 and 24hrs.

(G) Manders colocalization coefficient (MCC) M1 and M2, representing "Fraction TLR4 overlapping with Siglec-5" and "Fraction Siglec-5 overlapping with TLR4", respectively. Values were acquired from 4-7 images per slide.

(H) A panel of cytokines and chemokines was screened using the bio-plex assay in the supernatants of monocytes incubated for 24hrs with sialidase, with and without the TLR4 inhibitor TAK-242. Each datapoint is the mean of three biological replicates with three technical replicates pooled together.

Data is represented as mean±SD, statistical analysis was performed using one-way ANOVA with Dunnett's multiple comparisons test (*$p$<0.05; **$p$<0.01; ***$p$<0.001; ****$p$<0.0001).

**IL-6 secretion levels can be linked to distinct monocyte phenotypes**

The secretion of TLR4-dependent IL-6 production induced by sialidase, LPS, and M-CSF, was compared to monocytes stimulated with OA SFs using a sandwich ELISA. Sialidase and LPS induced the highest levels of IL-6 and OA SFs induced a low-grade inflammatory profile (Figure 6A).

By understanding how the patient IL-6 profiles corresponded to the phenotypes induced from the Siglec-5 – TLR4 interactions, clustering analysis was performed based on CD14, CD16, TLR4, Siglec-5, and Siglec-9. Clustering was performed on three biological replicates from monocytes stimulated with OA SF, whereas one biological replicate was used from the stimulations. All groups were downsampled to view 10.000 cells. Uniform Manifold Approximation and Projection (UMAP) dimensionality reduction (Figure 6B) displayed the six distinct monocyte populations generated (Pop1-Pop6), with Pop1 being the largest (71,100 cells) and Pop6 being the smallest (238 cells). Heatmap analysis of marker expression (Figure 6C) revealed that Pop1 was characterized by reduced TLR4/CD16 and increased Siglec-5/14/CD14 expression. Pop2 displayed the lowest levels of TLR4, accompanied by an induced CD14 expression. Siglec-5/14 was upregulated in Pop1, 3, 4, and 6. Each condition was displayed as UMAP density contour plots (Figure 6D). Pop1 and Pop4, along with Pop2 were the most abundant subtypes generated in monocytes stimulated with SF1-7, revealing similarities with the low-grade inflammatory profile induced by M-CSF. While monocytes stimulated with SFs displayed a wide distribution of subpopulations, it was evident that SF5 revealed similarities to the higher inflammatory conditions (LPS and sialidase) with a higher abundance of Pop3, Pop5, and Pop6 as well as a higher level of IL-6. These populations displayed the lowest expression of CD16, higher TLR4/CD14, and varying Siglec-5/14 levels.

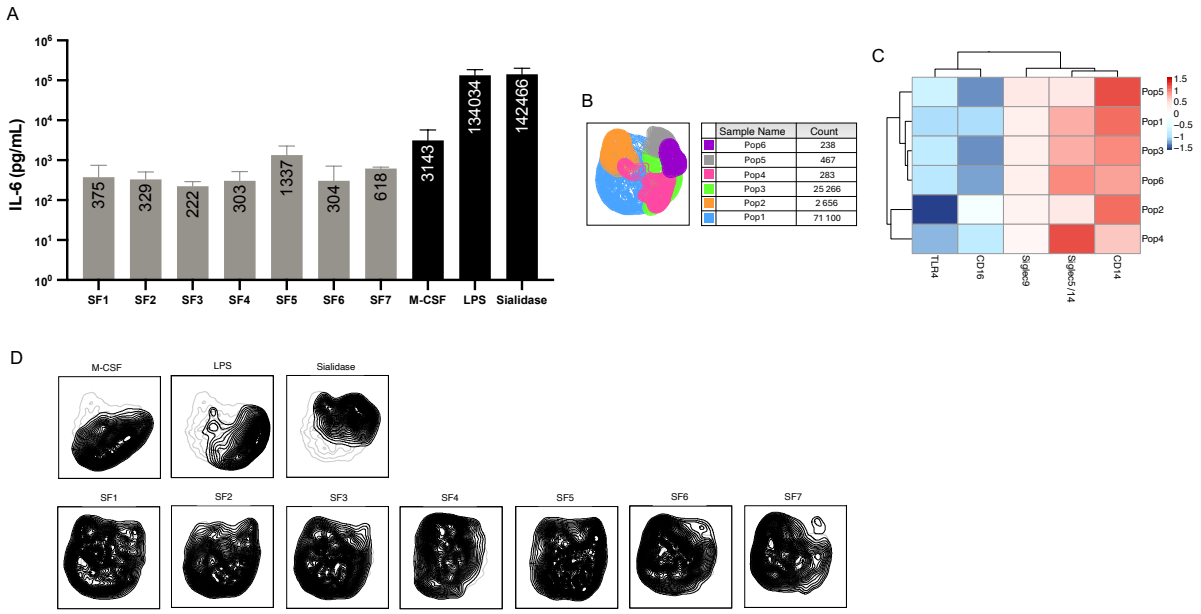


**Figure 6. IL-6 secretion levels can be linked to distinct monocyte phenotypes**

(A) The concentration of IL-6 (pg/mL) produced by the stimulated monocytes were quantified using a sandwich ELISA, grey bars represent SFs, and black bars represent the pathway-specific stimulations. Data is represented as mean±SD, with three technical replicates from three biological replicates.

(B) Analysis was performed on concatenated monocytes stimulated with M-CSF, LPS, sialidase, and SF1-7. Subsequently, monocytes were downsampled to 100,000 cells before performing clustering analysis using the FlowSOM plugin. This generated six monocyte subpopulations, the table displays each population and its count, respectively. For the monocytes stimulated with SF1-7, three technical replicates were used from three biological replicates. For monocytes stimulated with M-CSF, LPS, and sialidase, three technical replicates were used from one biological replicate.

(C) Heatmap analysis demonstrate the six populations and their relative expression of TLR4, CD16, Siglec-9, Siglec-5/14, and CD14.

(D) Each UMAP contour density plot represents one condition, i.e. M-CSF, LPS, sialidase, and SF1-7.

# DISCUSSION

In this study, we identified Siglec-5/14 as a potential regulatory protein in OA pathogenesis using a unique approach involving NPs. By performing proteomics analysis on the proteins formed around NPs incubated with OA SF, we detected Siglec-5/14 as one of 14 most abundant proteins. Through the IntAct Molecular Interaction Database, TLR4 was identified as the protein with the highest confidence score to Siglec-5 but not to Siglec-14. While the role of TLR4 has been extensively studied in OA, [22] the link to Siglecs remain unclear. We confirmed the regulatory role of Siglec-5/14 on monocytes by stimulating cells with OA SF,

476 inducing Siglec-5/14 expression which inversely correlated with TLR4. Mechanistically, we
477 showed that the potential Siglec-5 – TLR4 interactions are regulated by sialoglycans on the
478 cell surface, where highly inflammatory cytokines such as those induced by LPS or sialidase,
479 closely mirrored those found in patients with high inflammatory activity. Since TLR4 is
480 increasingly recognized as a key player in age-related diseases like OA, [22,23,27,47] our finding
481 that Siglec-5 can modulate TLR4-driven proinflammatory signaling highlights a potentially
482 unexplored regulatory axis in OA pathogenesis.
483
484 Interestingly, we found that OA SF induced Siglec-5/14 expression which inversely correlated
485 with TLR4 at 24hrs, suggesting potential crosstalk between these receptors. This inverse
486 relationship may reflect a negative feedback mechanism, where Siglec-5 reduces TLR4-
487 driven inflammation in OA, potentially mitigating tissue damage. To deduce Siglec-5-
488 mediated regulation of TLR4, SHP-1 was inhibited using TPI-1, and monocytes were
489 stimulated with LPS for 4hrs. Inhibition of SHP-1 resulted in an increased production of key
490 TLR4-associated cytokines, including IL-6, IL-8, and MCP-1, while levels of IL1β and TNFα
491 either decreased or remained the same. While these findings present some conflicting
492 patterns, they suggests Siglec-5 contributes to TLR4 regulation, with potentially more
493 pronounced effects at later timepoints. Siglec-5 has been shown to interact with TLR4, and
494 the murine Siglec-E facilitates TLR4 internalization. [21,32,48] Given that TLR4 is a key driver of
495 proinflammatory activity in OA, [22,47] its regulation by Siglec-5 may serve as an important
496 immunomodulatory checkpoint.
497 This was further strengthened by the observation that LPS and sialidase significantly reduced
498 TLR4 expression, likely as a desensitization mechanism to prevent monocytes from
499 overreacting to sustained inflammatory stimuli. [49] We investigated potential direct interactions
500 between the two receptors, as TLR4 is known to be heavily sialylated. [38,50] Using a Siglec-5
501 specific antibody, colocalization analysis revealed a strong overlap at baseline, in line with
502 previous studies suggesting that Siglecs can bind and regulate TLR activity. The high level of
503 IDRs at the membrane interface in both TLR4 and Siglec-5 indicate a tunable interaction
504 surface, one capable of rapid regulation in response to environmental cues, a key feature of
505 immune cell communication. [51]
506
507 However, with prolonged stimulations, we observed a progressive reduction in colocalization.
508 Colocalization scores below 0.2 indicated a loss of interaction, suggesting that LPS and
509 sialidase disrupted Siglec-5/TLR4 engagement. This supports a model where the interaction is
510 temporally regulated, strong early on then declining as immune activation progresses. This
511 temporal tuning may serve as a critical checkpoint, allowing for transient modulation of TLR4
512 signaling during early immune responses while ensuring desensitization under persistent
513 stimulation to prevent tissue damage.
514 Mechanistically, the loss of interaction appears to stem from depletion of membrane-bound
515 Sia rather than complete receptor downregulation. Surface Sia levels have been directly linked
516 to a cells' maturation state and inflammatory potential, [52,53] and their removal, via sialidase or
517 inflammatory stimuli, may directly influence Siglec binding. Both Siglec and TLR4
518 expression and activity are modulated by interactions with glycan structures, particularly α2,3

519 and α2,6 Sia linked residues. These glycan modifications can modulate immune cell signaling
520 and are often altered in response to inflammation [54,55].
521
522 The role of Siglec-5 in OA and its exact signaling mechanisms remain poorly understood. Our
523 study found that short-term activation reduced Siglec-5/14 expression, which was recovered
524 by 24hrs, suggesting either a shedding or internalization mechanism. A recent study on septic
525 patients found elevated levels of soluble Siglec-5 in plasma which could be induced by
526 stimulating monocytes with LPS. [17] Monocytes might hence shed Siglec-5 to modulate other
527 immune cells, explaining why Siglec-5 could be found in high abundance in the proteins
528 associated with the NPs. It is possible that Siglec-5 plays a role in this desensitization to not
529 exacerbate inflammation. Siglec-14, which has an opposing immunological role to Siglec-5,
530 has also been detected as a soluble protein, [20] however, the absence of changes in membrane
531 expression across different stimulations- when assessed using a Siglec-14-specific antibody,
532 suggests that the effect observed with the Siglec-5/14 targeting clone 1A5 are predominantly
533 driven by Siglec-5. Monocytes stimulated with LPS and sialidase exhibited highly similar
534 cytokine secretion profiles, reflecting their shared activation through TLR4. [37,38,56] Other
535 studies have shown that LPS leads to an overexpression of host sialidase, reducing
536 membrane-bound Sia, and using an exogenous sialidase can thereby mimic LPS stimulation.
537 [57] This functional similarity was further supported by the comparable inhibitory effects
538 observed by TAK-242. Several studies [36,58] have demonstrated changes in surface sialylation
539 in OA chondrocytes and fibroblast-like synoviocytes in rheumatoid arthritis, indicating that
540 inflammation significantly affects glycosylation patterns. [36,58] Our UMAP analysis revealed a
541 wide distribution of both low- and high-grade inflammatory monocytes, with
542 proinflammatory profiles generated by LPS and sialidase. Interestingly, SF5 exhibited an
543 overlap with a high-grade inflammatory profile, correlating with increased IL-6 secretion.
544 Other OA SF-stimulated monocytes shared similarities with M-CSF-stimulated monocytes,
545 consistent with a low-grade inflammation. These findings highlight how interpatient
546 variability influence subtle changes in monocyte surface markers, ultimately shaping
547 inflammatory responses, where Siglecs could play a role in regulation. The high levels of
548 Siglec-5 induced by LPS and contrasting low levels induced by sialidase, indicated that the
549 immunomodulatory effects by Siglec-5 was limited in high-inflammatory conditions within
550 24hrs. However, in low-grade inflammation, such as with OA SF, patients with higher Siglec-
551 5 expression may have a more tightly controlled immune response, preventing the
552 overactivation of TLR4 signaling and associated inflammation.
553
554 In conclusion, this study highlights the role of Siglec-5 on TLR4 in the pathogenesis of OA,
555 shedding light on their intricate interplay. While both Siglec-5 and TLR4 are implicated in the
556 inflammatory process of OA, their complex relationship warrants further investigation to fully
557 elucidate the underlying mechanisms and interactions and the contributing effects by Siglec-
558 14. The dynamic interplay between glycosylation, receptor localization, and immune
559 signaling could in the future be validated using proximity ligation assays, live cell imaging or
560 co-immunoprecipitation to further clarify the spatial and temporal nature of this interaction,
561 while lectin-based profiling could confirm changes in Sia presentation. The marked reduction
562 in cytokine production upon TLR4 inhibition underscores the therapeutic potential of TAK-

242 particularly for patient subgroups with low Siglec-5 or skewed Sia expression, where modulation of TLR4 signaling may prove especially beneficial. Similar features imposed on monocytes by LPS and sialidase demonstrated TLR4-specific activation. Yet, sialidase failed to upregulate Siglec-5, emphasizing an important role of Sia as ligand which could serve as a potential therapeutic target for immune cell modulation. Restoring Siglec-5 function and understanding its signaling mechanisms presents promising opportunities to modulate TLR4 signaling and reduce inflammation not only in OA, but for many pathogeneses where modulating glycosylation patterns can be used to fine-tune immune responses.

## Limitations of the study

We acknowledge some key limitations to our study. Employing an antibody that specifically recognizes Siglec-5 would help avoid ambiguity arising from cross-reactivity with Siglec-14, as is possible with the 1A5 clone. While this study has focused on healthy monocytes, many different cells are involved in OA, including chondrocytes and synoviocytes. Modulation of $CD8^+$ T-cell proliferation by soluble Siglec-5, [17] suggests Siglec-5 could have potential effects on other OA-related cells. The transient increases in Siglec-5, alongside persistent decreases in the sialidase group, suggest ongoing glycan remodeling that may involve TLR4 or other receptors. Longer observation periods and dose-dependent studies, particularly with sialidase, are needed to clarify these dynamics. Broader investigation into glycosylation patterns and their impact on immune receptor networks could uncover additional therapeutic targets. Future work should also validate these findings in vivo and in human OA samples, particularly OA-derived monocytes, focusing on how sialylation patterns and Siglec-5 expression vary among patient subgroups.

## Resource availability

### Lead contact

Further information and requests for resources should be directed to and will be fulfilled by the lead contact, Alexandra Stubelius (alexandra.stubelius@chalmers.se).

### Material availability

The study did not generate new materials.

### Data and code availability

- All data can be obtained from the lead contact, provided the request is reasonable.
- The code related to the algorithm can be accessed by reaching out to the lead contact.
- Any additional information required to reanalyze the data reported in this paper is available from the lead contact upon request.

## Acknowledgements

Anna-Karin Hultgård-Ekwall, Lena Björkman, Thomas Eisler, and Ola Rolfson are gratefully acknowledged for arranging the patient samples, and Sofia Grindberg and Paula-Therese Kelly Pettersson at Danderyd's Hospital and Lotta Falkendahl at the University of Gothenburg are acknowledged for their assistance in collecting the samples. This work was supported by

Chalmers Technical University and its Area of Advance Nano. The authors greatly acknowledge further financial support from the Foundation for Sigurd and Elsa Goljes Minne (LA2021-0100), The Royal Swedish Academy of Sciences (CR2021-0024), The Jeanssons Foundation (J2021-0050), The Hasselblad Foundation, the Swedish Research Council (2021-01870), Wilhelm och Martina Lundgrens Vetenskapsfond (2022-4054) the Swedish Rheumatism Association (R-981253), the King Gustav V's 80 years' foundation (FAI-2022-0872) and IngaBritt och Arne Lundbergs Forskningsstiftelse (LU2022-0041).

## Author Contributions

Study design (L.R, A.S), conducting experiments (L.R, F.J, U.v.M, V.V), acquiring data (L.R, F.J, U.v.M, V.V), analyzing data (L.R, F.J, U.v.M, V.V, A.S), providing funding and reagents (N.K, A,S), writing the manuscript (L.R, A.S). All authors have contributed to editing and approved the manuscript.

## Declaration of interest

NK authored a patent involving OA diagnostics, and NK hold equity in Lynxon AB. The other authors have declared that no conflict of interest exists.

## Declaration of generative AI and AI-assisted technologies in the writing process

During the preparation of this work, we used OpenAI for language editing and to ensure readability. After using this tool/service, we reviewed and edited the content and take full responsibility for the content of the published article.

# STAR METHODS

## EXPERIMENTAL MODEL AND STUDY PARTICIPANT DETAILS

### Sex as a biological variable

This study includes patient material from both female and male patients. Synovial fluid from 7 OA patients (2 females) due for total knee replacement surgery was selected for the experiments: age 63-87 (Median 77) and BMI 23.4-38.0 (Median 25.6). Due to the small patient population, no further stratification was made. To remove cells from OA SF, the SFs were centrifuged at 3000 x g for 10 min before being stored at -80°C.

### Primary cultures

Buffy coats were obtained from anonymous healthy donors from the blood bank at Sahlgrenska University Hospital, Gothenburg, Sweden (18/23). The sex of the cells could not be reported as they were obtained from anonymous donors. Isolated cells were cultured at 37°C with 5% $CO_2$.

648 **METHOD DETAILS**
649
650 **Protein corona isolation and material synthesis**
651 NP synthesis was previously described in von Mentzer *et al.* [10] Briefly, PAMAM (G5) were
652 modified by PEGylation using PEG 350 MW, $NP_{350}$ at 2%, or PEG 5000 MW, $NP_{5000}$ at 2%,
653 purified, and used at the final concentration of 30 µM in PBS (pH = 7.4).
654
655 SF samples from 4 (2f/2m, 45–82 years old) late OA patients were collected during aseptic
656 aspiration of knee joints at the Rheumatology Clinic and Orthopaedic Clinic, respectively, at
657 Sahlgrenska University Hospital, Gothenburg, Sweden.
658 Patient SF were pooled, diluted 1:20 in PBS, and mixed with 30 µM NP solution (1:1, v/v).
659 The samples were incubated at 37°C while shaking for 1 h at 100 rpm to resemble the
660 dynamic environment of the SF in the joint and address the Vroman effect. To preserve the
661 proteins bound with high affinity known as the hard protein coronas, NPs were spun down at
662 15,000 × *g* for 15 min and washed three times with chilled PBS. Final concentration of NP-
663 protein complexes was 1 µg/mL ($2.5 \times 10^8$ particles/mL).
664
665 NPs were pelleted by centrifugation at 15,000 × *g* for 15 min, snap-frozen using liquid
666 nitrogen, and submitted to the Proteomics Core Facility (Gothenburg, Sweden). Briefly,
667 proteins were digested into peptides using MS-grade trypsin and analyzed by nanoscale liquid
668 chromatography-tandem mass spectrometry LC-MS/MS. The mascot search engine was used
669 to match the discovered peptide sequences against SwissProt human and bovine protein
670 database using Proteome Discoverer. Data were analyzed using a label-free quantification
671 method and the protein false discovery rate was set to 1%. To elucidate the molecular
672 functions and classifications of significant proteins, the enrichment analysis was performed
673 using Gene Ontology-based PANTHER classification system. SF samples were matched to
674 human (Homo sapiens). The detected proteins were analyzed and illustrated as a volcano plot
675 using the DEP R package as described in. [10]
676
677 **Monocyte isolation**
678 Buffy coats were prepared at Sahlgrenska hospital the day before and collected for the
679 experimental study in the morning. Monocyte isolation was performed using the negative
680 selection RosettSep™ Human Monocyte Enrichment Cocktail. Since this kit is optimized for
681 whole blood, the buffy coat was diluted 1:1 with Dulbecco's phosphate buffered saline (PBS)
682 (Gibco) to ensure that the concentration of nucleated cells did not exceed the limit. Apart
683 from that, the isolation was performed according to the protocol. The blood:PBS was mixed
684 with the cocktail and 1mM EDTA and incubated for 20 min at room temperature. Following
685 this, the mixture was placed over a Lymphoprep™ density gradient medium and centrifuged
686 in a swing-out bucket for 20 min at 1200 x g with the brake off. The enriched monocytes were
687 transferred to a new tube and washed in the recommended medium containing PBS, 2% heat
688 inactivated fetal bovine serum (FBS) and 1mM EDTA. The monocytes were washed three
689 times in recommended medium and centrifuged at 300 x g for 10 min with the brake low for
690 the first two washes. For the final wash step, the cells were centrifuged for 120 x g for 10 min
691 with the brake off to remove platelets.

692
693 **Monocyte stimulations**
694 The enriched monocytes were counted and plated at a concentration of 3 x $10^5$ cells/well in a
695 48 well plate. The cells were diluted in RPMI Medium supplemented with 1 % glutaMAX, 1
696 % Penicillin/Streptomycin and 10 % FBS. TAK-242 or TPI-1 was added to the designated
697 wells at a concentration of 1µM or 100ng/mL, respectively, and incubated for one hour. The
698 final concentration of each stimulation was 10ng/mL of IL1β and TNFα, 100ng/mL M-CSF,
699 100ng/mL LPS, and 100mU/mL sialidase. The total volume per well was 250µL. The cells
700 were analyzed after 0, 4, and 24 hours.
701 As a comparison to these commonly used stimulations, we incubated primary monocytes with
702 OA synovial fluid at a concentration of 25%. After 24hrs of stimulation the surface markers
703 were detected using flow cytometry.
704
705 **Cell staining for flow cytometric analysis**
706 Monocytes were collected by transferring the whole volume to a v-plate and centrifuging
707 them at 300 x g for 5 minutes, 4°C. The supernatants were transferred and saved at -80°C for
708 cytokine measurement. Meanwhile, to detach the monocytes that started differentiating into
709 macrophages, 50µL trypsin-EDTA was added. Once detached, 50µL ice cold recommended
710 medium was used to inactivate trypsin. The detached cells were added to the v-plate and
711 washed twice. 10µL Fc block was added to each well and the plate was incubated on ice for
712 10 min. Monocyte phenotypes were analyzed using the following antibodies at a final
713 concentration of 1:100, CD14-FITC, CD16-Brilliant Violet 605, Siglec-5-PE, Siglect-9-PE-
714 Cy7, and TLR4-APC. 10µL the antibody cocktail was added to each well and the plate was
715 incubated for 20 min on ice in the dark. UltraComp eBeads™ Plus Compensation Beads were
716 used to compensate spillover. The cells and compensation beads were washed three times in
717 recommended medium. To exclude dead cells, 3µM DAPI was added. Fluorescence minus
718 one (FMO) and unstained cells were used to set up the gating for each individual experiment.
719 The cells were run on the Cytoflex LX (Beckman Coulter), median fluorescence intensity
720 (MFI) was recorded and analyzed using FlowJo (Version 10.10.0). [59]
721
722 **Unsupervised flow cytometric analysis**
723 Unsupervised analysis was performed using FlowJo. Cells from all stimulations (SF1-SF7 and
724 M-CSF, LPS, and sialidase) were concatenated into one single file. Clustering was conducted
725 using the FlowSOM plugin, generating six distinct populations. Subsequently, a UMAP was
726 generated based on these populations. For visualization, each stimulation condition was
727 overlaid onto separate UMAPs to illustrate the distribution of populations across each
728 stimulation.
729
730 **LC-MS**
731 After isolating monocytes, they were diluted to a concentration of 2 x $10^6$ cells and added to
732 two Eppendorf tubes. Sialidase was added so that the number of units per cell was the same as
733 in the experiments, the tubes were incubated for 1 hour at 37°C. The tubes were centrifuged at
734 2500 x g for 10 min at 4°C. Supernatant was removed, the same washing step was performed
735 two more times. Subsequently, 100µL lysis buffer (PBS + 2% SDS) was added, the tubes

736 were briefly sonicated followed by gentle shaking for 10 min. Cell debris was removed by
737 centrifugation at 14000 x g for 20 min. The supernatant was collected, and the protein
738 concentration was measured using gold-standard BCA assay. Approximately 30 µg of
739 extracted protein samples were dot blotted on a PVDF membrane (Millipore). Proteins were
740 stained using Alcian blue stain solution, excised and transferred to an Eppendorf tube.
741 O-glycans were released and analyzed on liquid chromatography and mass spectrometry
742 according to this protocol. In short, the dot blotted proteins were subjected to reductive β-
743 elimination with 0.5 M sodium borohydride in 50 mM sodium hydroxide for 16 h at 50°C to
744 release the glycans. The reduction reaction was quenched by the addition of glacial acetic acid
745 and the resulting glycan containing mixtures were desalted using strong cation exchange resin
746 packed on top of C18 column to remove the remaining proteins or peptides. The released
747 glycans were analyzed using liquid chromatography and mass spectrometry. The glycans
748 were separated on a column (10 cm × 250 µm) packed in-house with 5 µm porous graphite
749 particles (PGC, Hypercarb, Thermo-Hypersil, Runcorn, UK) and at a flow rate of 6 µl/min.
750 The samples were analyzed in negative ion mode on an Orbitrap mass spectrometer (Fusion,
751 Thermo Electron, San José, CA) and the data acquisition was conducted with Xcalibur
752 software (Version 2.0.7).
753
754 **Bio-Plex Pro Human Cytokine Panel 27-Plex**
755 Supernatants from the monocyte stimulation assays were screened for a panel of 27 cytokines
756 and chemokines to evaluate the immune response in the different conditions. The technical
757 replicates from three biological replicates were combined, respectively, to reduce the number
758 of wells to one well per biological replicate. The assay was performed according to the
759 manufacturer's instructions. Vortexed beads were added to each well, followed by two
760 washing steps. The supernatants were centrifuged at 1,000 x g for 15 min at 4°C prior being
761 added to the plate along with the standard, blank, and control. The plate was incubated
762 shaking at 850 rpm for 30 min, followed by three washing steps. Detection antibodies were
763 added to each well and incubated shaking for 30 min. After three washings, streptavidin-PE
764 was added and incubated shaking for 10 min. An additional three washings were performed
765 before resuspending the beads in assay buffer and reading the plate.
766 For values that were out of range, extrapolated values were assumed based on the highest and
767 lowest value of the standard curve. We observed that most of the groups was below detection
768 level for IL-7 and above detection level for MIP-1α, MIP-1β, IL-6, and IL-8 and they were
769 hence removed. Additionally, the media control was below detection level for most analytes
770 and thus removed.
771
772 The cytokines detected were normalized in Prism (GraphPad software Version 10.4.1 (532)).
773 For each subcolumn, values were scaled as fractions, with 0% representing smallest value of
774 each sub column, and 100% represents the sum of all values in the subcolumn. The ggplot2
775 R[60] package was used to create the dot plot heatmap illustrating cytokine expression under
776 different stimulation conditions, along with the percentage cytokines remaining in presence of
777 TAK-242.
778
779 **IL-6 ELISA**

780 To determine the quantity of IL-6 in the supernatants of monocytes stimulated with SFs and
781 M-CSF, LPS, and sialidase, a sandwich ELISA was performed according to the
782 manufacturer's protocol. Briefly, the ELISA plate was coated with the capture antibody the
783 day before and incubated overnight the fridge. In the morning the next day, the plate was
784 washed four times and blocked for 1 hour, shaking at 500rpm. Meanwhile, the standard and
785 sample dilutions were prepared and subsequently added after an additional four washes. The
786 plate was incubated for 2 hours, shaking, then washed four times. Detection antibody was
787 added, and the plate was incubated for 1 hour, shaking. The same washing procedure was
788 performed and avidin-HRP was added and incubated for 30 min, shaking. After this, the plate
789 was washed 5 times and TMB substrate solution (A+B) was added and incubated for 15 min
790 in the dark. Stop solution was added and the absorbance at 450nm and 570nm was detected.
791
792 **LEGENDplex Human Inflammation Panel 1 (13-plex)**
793 A panel of 13 cytokines were screened in the supernatants of monocytes stimulated for 4hrs
794 with and without the TPI-1 inhibitor. Following the manufacturer's instructions, assay buffer,
795 sample, standard, and premixed beads were added to a v-bottom plate and incubated for 2hrs
796 shaking at room temperature at 800 rpm in the dark. Two washed was performed by
797 centrifuging at 250 x g for 5 min. The supernatant was removed by flicking the plate.
798 Detection antibodies was added and the plate was incubated for 1hrs, at room temperature at
799 800rpm, in the dark. SA-PE was added and the plate incubated for an additional 30 min.
800 Following this, the plate was washed twice and the beads were resuspended in wash buffer
801 and detected on the Cytoflex LX (Beckman Coulter) and analyzed on Biolegends
802 LEGENDplex software.
803
804 **Confocal microscopy**
805 To analyze TLR4 and Siglec-5 colocalization, confocal imaging was performed. $1.2x10^6$
806 isolated monocytes were seeded in complete RPMI in 12 well plates and pre-treated with
807 1µM TAK-242 or PBS, for 1 hour. Following this, the stimulations M-CSF, LPS, and
808 Sialidase were added accorded to previously mentioned concentrations. After 0 and 24h, the
809 monocytes were transferred to Eppendorf tubes and the leftover attached cells were
810 trypsinized and transferred to the tubes before being centrifuged at 1,500 rpm for 5 min. The
811 supernatant was discarded, and the cells were washed with PBS and centrifuged to remove the
812 supernatant, this was performed three times. To fix the cells, 100µL 4% paraformaldehyde
813 was added to each tube and incubated at room temperature for 10 min. The monocytes were
814 blocked for 30 min with 5% FBS. Detection was performed using anti-human TLR4 mouse
815 monoclonal antibody and anti-human Siglec-5 rabbit polyclonal antibody, both diluted 1:100
816 and stained for 1h in room temperature. 2 µg/mL of secondary antibody goat anti-mouse IgG
817 and goat anti-rabbit IgG was incubated in the dark for 1h. After washing, the cells were spun
818 onto a glass slide, ProLong™ Gold Antifade Mountant was added before mounting the cover
819 slip.
820
821 To verify sialidase enzyme efficiency at 24hrs in culture, $1.2x10^6$ isolated monocytes were
822 seeded in complete RPMI in 12 well plates with or without the enzyme. The fixation protocol
823 was the same as above, with a few exceptions; blocking was performed for 30 min using

carbo-free buffer. For detecting Sia, lectin staining was performed using 10µg/mL Maackia Amurensis-I (MAL-1)-FITC and 10µg/mL Sambucus Nigra (SNA)-Cy5, targeting α2,3 and α2,6 Sia, respectively.

Images were acquired by using an inverted Nikon C2+ confocal microscope (Nikon Instruments, Amsterdam, Netherlands) equipped with a C2-DUVB GaAsP detector unit offering variable emission bandpass settings. A 60x Nikon APO oil-immersion objective (numerical aperture 1.4). Excitation and emission were set as follows for different staining: DAPI - $\lambda_{ex}$ 401 nm, $\lambda_{em}$ 425-497 nm, goat anti-rabbit IgG (Alexa Fluor 647) - $\lambda_{ex}$ 639 nm, $\lambda_{em}$ 644-695 nm, goat anti-mouse IgG (Alexa Fluor 488) - $\lambda_{ex}$ 489 nm, $\lambda_{em}$ 503-546 nm, MAL-I (FITC) - $\lambda_{ex}$ 489 nm, $\lambda_{em}$ 513-544 nm, and SNA (Cy5) - $\lambda_{ex}$ 639 nm, $\lambda_{em}$ 646-689 nm.

**Image analysis**

The confocal images displayed in Figure 4A were enhanced for illustrative purposes. The brightness was equally enhanced for TLR4 and Siglec-5, for accurate comparison. Mander's colocalization coefficient (MMC) was performed on unaltered images. Threshold was set to 90 for TLR4 and 140 for Siglec-5 to remove background. Antibody validation was performed to evaluate cross-species binding, these controls demonstrated 0 overlap. MCC was calculated through the JACoP plugin in ImageJ2 (Version 2.16.0/1.54p). [61]

Quantification of α2,3 and α2,6 Sia was performed by extracting the MFI from the original intensity profiles with no alterations.

**Protein prediction**

The protein prediction was analyzed and saved using ChimeraX. [62]

**R packages**

Figure 1B, Figure 4A, Figure 6C, and Figure S7A were created in Rstudio (R version 4.3.2 (2023-10-31). The following packages were used: readr, tidyverse, igraph, ggraph, ggplot2, and scales.[63-69]

**Statistics**

Statistical significance was performed using Prism (GraphPad software Version 10.4.1 (532)). Data are shown as the mean and standard deviation and statistical differences were analyzed using One-way ANOVA followed by Tukey's or Dunnett's multiple comparisons test or two-way ANOVA followed by Sidak's multiple comparisons test. Correlation was analyzed using Spearman correlation analysis. All statistical details can be obtained in the figure legends.

**Study approval**

The studies involving human participants were reviewed and approved by the Regional Ethical Review Board in Gothenburg. All patients provided informed consent, and the procedure was approved by the Ethics Committee of Gothenburg University (Ethical approval Dnr: 573-07, 172-15).

# References


1. Courties, A., Kouki, I., Soliman, N., Mathieu, S., and Sellam, J. (2024). Osteoarthritis year in review 2024: Epidemiology and therapy. Osteoarthritis Cartilage *32*, 1397-1404. 10.1016/j.joca.2024.07.014.
2. Ye, Z., Wang, Y., Xiang, B., Wang, H., Tao, H., Zhang, C., Zhang, S., Sun, D., Luo, F., and Song, L. (2023). Roles of the Siglec family in bone and bone homeostasis. Biomed Pharmacother *165*, 115064. 10.1016/j.biopha.2023.115064.
3. Zhang, H., Cai, D., and Bai, X. (2020). Macrophages regulate the progression of osteoarthritis. Osteoarthritis and Cartilage *28*, 555-561. 10.1016/j.joca.2020.01.007.
4. Zhu, X., Lee, C.-W., Xu, H., Wang, Y.-F., Yung, P.S.H., Jiang, Y., and Lee, O.K. (2021). Phenotypic alteration of macrophages during osteoarthritis: a systematic review. Arthritis Research & Therapy *23*. 10.1186/s13075-021-02457-3.
5. Yin, X., Wang, Q., Tang, Y., Wang, T., Zhang, Y., and Yu, T. (2024). Research progress on macrophage polarization during osteoarthritis disease progression: a review. Journal of Orthopaedic Surgery and Research *19*. 10.1186/s13018-024-05052-9.
6. Kloppenburg, M., Peterfy, C., Haugen, I.K., Kroon, F., Chen, S., Wang, L., Liu, W., Levy, G., Fleischmann, R.M., Berenbaum, F., et al. (2019). Phase IIa, placebo-controlled, randomised study of lutikizumab, an anti-interleukin-1α and anti-interleukin-1β dual variable domain immunoglobulin, in patients with erosive hand osteoarthritis. Annals of the Rheumatic Diseases *78*, 413-420. 10.1136/annrheumdis-2018-213336.
7. Yu, L., Luo, R., Qin, G., Zhang, Q., and Liang, W. (2023). Efficacy and safety of anti-interleukin-1 therapeutics in the treatment of knee osteoarthritis: a systematic review and meta-analysis of randomized controlled trials. Journal of Orthopaedic Surgery and Research *18*. 10.1186/s13018-023-03590-2.
8. Zhu, R., Fang, H., Wang, J., Ge, L., Zhang, X., Aitken, D., and Cai, G. (2024). Inflammation as a therapeutic target for osteoarthritis: A literature review of clinical trials. Clinical Rheumatology *43*, 2417-2433. 10.1007/s10067-024-07042-y.
9. Morici, L., Allémann, E., Rodríguez-Nogales, C., and Jordan, O. (2024). Cartilage-targeted drug nanocarriers for osteoarthritis therapy. Int J Pharm *666*, 124843. 10.1016/j.ijpharm.2024.124843.
10. von Mentzer, U., Sellden, T., Raberg, L., Erensoy, G., Hultgard Ekwall, A.K., and Stubelius, A. (2022). Synovial fluid profile dictates nanoparticle uptake into cartilage - implications of the protein corona for novel arthritis treatments. Osteoarthritis Cartilage *30*, 1356-1364. 10.1016/j.joca.2022.07.002.
11. Angata, T., Hayakawa, T., Yamanaka, M., Varki, A., and Nakamura, M. (2006). Discovery of Siglec-14, a novel sialic acid receptor undergoing concerted evolution with Siglec-5 in primates. The FASEB Journal *20*, 1964-1973. 10.1096/fj.06-5800com.
12. Vuchkovska, A., Glanville, D.G., Scurti, G.M., Nishimura, M.I., White, P., Ulijasz, A.T., and Iwashima, M. (2022). Siglec-5 is an inhibitory immune checkpoint molecule for human T cells. Immunology *166*, 238-248. 10.1111/imm.13470.
13. Läubli, H., Nalle, S.C., and Maslyar, D. (2022). Targeting the Siglec–Sialic Acid Immune Axis in Cancer: Current and Future Approaches. Cancer Immunology Research *10*, 1423-1432. 10.1158/2326-6066.cir-22-0366.
14. Lustig, M., Chan, C., Jansen, J.H.M., Bräutigam, M., Kölling, M.A., Gehlert, C.L., Baumann, N., Mester, S., Foss, S., Andersen, J.T., et al. (2023). Disruption of the sialic acid/Siglec-9 axis improves antibody-mediated neutrophil cytotoxicity towards tumor cells. Frontiers in Immunology *14*. 10.3389/fimmu.2023.1178817.

15. Wang, X., Liu, D., Ning, Y., Liu, J., Wang, X., Tu, R., Shen, H., Chen, Q., and Xiong, Y. (2017). Siglec-9 is upregulated in rheumatoid arthritis and suppresses collagen-induced arthritis through reciprocal regulation of Th17-/Treg-cell differentiation. Scand J Immunol *85*, 433-440. 10.1111/sji.12543.
16. Dou, C., Zhen, G., Dan, Y., Wan, M., Limjunyawong, N., and Cao, X. (2022). Sialylation of TLR2 initiates osteoclast fusion. Bone Research *10*, 24. 10.1038/s41413-022-00186-0.
17. Lozano-Rodríguez, R., Avendaño-Ortíz, J., Montalbán-Hernández, K., Ruiz-Rodríguez, J.C., Ferrer, R., Martín-Quirós, A., Maroun-Eid, C., González-López, J.J., Fàbrega, A., Terrón-Arcos, V., et al. (2023). The prognostic impact of SIGLEC5-induced impairment of CD8+ T cell activation in sepsis. eBioMedicine *97*, 104841. 10.1016/j.ebiom.2023.104841.
18. Kukan, E.N., Fabiano, G.L., and Cobb, B.A. (2024). Siglecs as modulators of macrophage phenotype and function. Semin Immunol *73*, 101887. 10.1016/j.smim.2024.101887.
19. Matsumoto, T., Takahashi, N., Kojima, T., Yoshioka, Y., Ishikawa, J., Furukawa, K., Ono, K., Sawada, M., Ishiguro, N., and Yamamoto, A. (2016). Soluble Siglec-9 suppresses arthritis in a collagen-induced arthritis mouse model and inhibits M1 activation of RAW264.7 macrophages. Arthritis Res Ther *18*, 133. 10.1186/s13075-016-1035-9.
20. Huang, P.-C.J., Low, P.-Y., Wang, I., Hsu, S.-T.D., and Angata, T. (2018). Soluble Siglec-14 glycan-recognition protein is generated by alternative splicing and suppresses myeloid inflammatory responses. Journal of Biological Chemistry *293*, 19645-19658. 10.1074/jbc.ra118.005676.
21. Wu, Y., Ren, D., and Chen, G.-Y. (2016). Siglec-E Negatively Regulates the Activation of TLR4 by Controlling Its Endocytosis. The Journal of Immunology *197*, 3336-3347. 10.4049/jimmunol.1600772.
22. Bartels, Y.L., Van Lent, P.L.E.M., Van Der Kraan, P.M., Blom, A.B., Bonger, K.M., and Van Den Bosch, M.H.J. (2024). Inhibition of TLR4 signalling to dampen joint inflammation in osteoarthritis. Rheumatology *63*, 608-618. 10.1093/rheumatology/kead493.
23. Kim, H.-J., Kim, H., Lee, J.-H., and Hwangbo, C. (2023). Toll-like receptor 4 (TLR4): new insight immune and aging. Immunity & Ageing *20*. 10.1186/s12979-023-00383-3.
24. Rapp, A.E., and Zaucke, F. (2023). Cartilage extracellular matrix-derived matrikines in osteoarthritis. Am J Physiol Cell Physiol *324*, C377-C394. 10.1152/ajpcell.00464.2022.
25. von Mentzer, U., Corciulo, C., and Stubelius, A. (2022). Biomaterial Integration in the Joint: Pathological Considerations, Immunomodulation, and the Extracellular Matrix. Macromol Biosci *22*, e2200037. 10.1002/mabi.202200037.
26. Huang, S., Thomsson, K.A., Jin, C., Ryberg, H., Das, N., Struglics, A., Rolfson, O., Björkman, L.I., Eisler, T., Schmidt, T.A., et al. (2022). Truncated lubricin glycans in osteoarthritis stimulate the synoviocyte secretion of VEGFA, IL-8, and MIP-1α: Interplay between O-linked glycosylation and inflammatory cytokines. Frontiers in Molecular Biosciences *9*. 10.3389/fmolb.2022.942406.
27. Gómez, R., Villalvilla, A., Largo, R., Gualillo, O., and Herrero-Beaumont, G. (2015). TLR4 signalling in osteoarthritis—finding targets for candidate DMOADs. Nature Reviews Rheumatology *11*, 159-170. 10.1038/nrrheum.2014.209.
28. Barreto, G., Senturk, B., Colombo, L., Brück, O., Neidenbach, P., Salzmann, G., Zenobi-Wong, M., and Rottmar, M. (2020). Lumican is upregulated in osteoarthritis and contributes to TLR4-induced pro-inflammatory activation of cartilage degradation and

966 macrophage polarization. Osteoarthritis and Cartilage *28*, 92-101.
967 10.1016/j.joca.2019.10.011.
968 29. Barreto, G., Manninen, M., and K. Eklund, K. (2020). Osteoarthritis and Toll-
969 Like Receptors: When Innate Immunity Meets Chondrocyte Apoptosis. Biology *9*, 65.
970 10.3390/biology9040065.
971 30. Tsuno, H., Tanaka, N., Naito, M., Ohashi, S., Iwasawa, M., Kadoguchi, T.,
972 Mitomi, H., Matsui, T., Furukawa, H., and Fukui, N. (2023). Analysis of proteins released
973 from osteoarthritic cartilage by compressive loading. Scientific Reports *13*. 10.1038/s41598-
974 023-45472-x.
975 31. Warmink, K., Vinod, P., Korthagen, N.M., Weinans, H., and Rios, J.L. (2023).
976 Macrophage-Driven Inflammation in Metabolic Osteoarthritis: Implications for Biomarker
977 and Therapy Development. International Journal of Molecular Sciences *24*, 6112.
978 10.3390/ijms24076112.
979 32. Chen, G.Y., Brown, N.K., Wu, W., Khedri, Z., Yu, H., Chen, X., van de
980 Vlekkert, D., D'Azzo, A., Zheng, P., and Liu, Y. (2014). Broad and direct interaction
981 between TLR and Siglec families of pattern recognition receptors and its regulation by
982 Neu1. Elife *3*, e04066. 10.7554/eLife.04066.
983 33. Feng, C., Stamatos, N.M., Dragan, A.I., Medvedev, A., Whitford, M., Zhang, L.,
984 Song, C., Rallabhandi, P., Cole, L., Nhu, Q.M., et al. (2012). Sialyl residues modulate LPS-
985 mediated signaling through the Toll-like receptor 4 complex. PLoS One *7*, e32359.
986 10.1371/journal.pone.0032359.
987 34. Wang, T., Hao, Z., Liu, C., Yuan, L., Li, L., Yin, M., Li, Q., Qi, Z., and Wang,
988 Z. (2020). MiR-193b modulates osteoarthritis progression through targeting ST3GAL4 via
989 sialylation of CD44 and NF-κB pathway. Cell Signal *76*, 109814.
990 10.1016/j.cellsig.2020.109814.
991 35. Liang, F., Seyrantepe, V., Landry, K., Ahmad, R., Ahmad, A., Stamatos, N.M.,
992 and Pshezhetsky, A.V. (2006). Monocyte Differentiation Up-regulates the Expression of the
993 Lysosomal Sialidase, Neu1, and Triggers Its Targeting to the Plasma Membrane via Major
994 Histocompatibility Complex Class II-positive Compartments. Journal of Biological
995 Chemistry *281*, 27526-27538. 10.1074/jbc.m605633200.
996 36. Carpintero-Fernandez, P., Varela-Eirin, M., Lacetera, A., Gago-Fuentes, R.,
997 Fonseca, E., Martin-Santamaria, S., and Mayan, M.D. (2020). New Therapeutic Strategies
998 for Osteoarthritis by Targeting Sialic Acid Receptors. Biomolecules *10*, 637.
999 10.3390/biom10040637.
1000 37. Allendorf, D.H., Franssen, E.H., and Brown, G.C. (2020). Lipopolysaccharide
1001 activates microglia via neuraminidase 1 desialylation of Toll-like Receptor 4. Journal of
1002 Neurochemistry *155*, 403-416. 10.1111/jnc.15024.
1003 38. Karmakar, J., Roy, S., and Mandal, C. (2019). Modulation of TLR4 Sialylation
1004 Mediated by a Sialidase Neu1 and Impairment of Its Signaling in Leishmania donovani
1005 Infected Macrophages. Frontiers in Immunology *10*. 10.3389/fimmu.2019.02360.
1006 39. Barreto, G., Sandelin, J., Salem, A., Nordström, D.C., and Waris, E. (2017).
1007 Toll-like receptors and their soluble forms differ in the knee and thumb basal osteoarthritic
1008 joints. Acta Orthopaedica *88*, 326-333. 10.1080/17453674.2017.1281058.
1009 40. Huang, Z.Y., Perry, E., Huebner, J.L., Katz, B., Li, Y.-J., and Kraus, V.B.
1010 (2018). Biomarkers of inflammation – LBP and TLR— predict progression of knee
1011 osteoarthritis in the DOXY clinical trial. Osteoarthritis and Cartilage *26*, 1658-1665.
1012 10.1016/j.joca.2018.08.005.
1013 41. Villaveces, J.M., Jimenez, R.C., Porras, P., Del-Toro, N., Duesbury, M.,
1014 Dumousseau, M., Orchard, S., Choi, H., Ping, P., Zong, N.C., et al. (2015). Merging and

scoring molecular interactions utilising existing community standards: tools, use-cases and a case study. Database *2015*, bau131-bau131. 10.1093/database/bau131.

42. Gómez-Aristizábal, A., Gandhi, R., Mahomed, N.N., Marshall, K.W., and Viswanathan, S. (2019). Synovial fluid monocyte/macrophage subsets and their correlation to patient-reported outcomes in osteoarthritic patients: a cohort study. Arthritis Research & Therapy *21*. 10.1186/s13075-018-1798-2.

43. Kapellos, T.S., Bonaguro, L., Gemünd, I., Reusch, N., Saglam, A., Hinkley, E.R., and Schultze, J.L. (2019). Human Monocyte Subsets and Phenotypes in Major Chronic Inflammatory Diseases. Frontiers in Immunology *10*. 10.3389/fimmu.2019.02035.

44. Williams, H., Mack, C., Baraz, R., Marimuthu, R., Naralashetty, S., Li, S., and Medbury, H. (2023). Monocyte Differentiation and Heterogeneity: Inter-Subset and Interindividual Differences. International Journal of Molecular Sciences *24*, 8757. 10.3390/ijms24108757.

45. Abramson, J., Adler, J., Dunger, J., Evans, R., Green, T., Pritzel, A., Ronneberger, O., Willmore, L., Ballard, A.J., Bambrick, J., et al. (2024). Accurate structure prediction of biomolecular interactions with AlphaFold 3. Nature *630*, 493-500. 10.1038/s41586-024-07487-w.

46. Takashima, K., Matsunaga, N., Yoshimatsu, M., Hazeki, K., Kaisho, T., Uekata, M., Hazeki, O., Akira, S., Iizawa, Y., and Ii, M. (2009). Analysis of binding site for the novel small-molecule TLR4 signal transduction inhibitor TAK-242 and its therapeutic effect on mouse sepsis model. Br J Pharmacol *157*, 1250-1262. 10.1111/j.1476-5381.2009.00297.x.

47. Kalaitzoglou, E., Lopes, E.B.P., Fu, Y., Herron, J.C., Flaming, J.M., Donovan, E.L., Hu, Y., Filiberti, A., Griffin, T.M., and Humphrey, M.B. (2019). TLR4 Promotes and DAP12 Limits Obesity-Induced Osteoarthritis in Aged Female Mice. JBMR Plus *3*, e10079. 10.1002/jbm4.10079.

48. Boyd, C.R., Orr, S.J., Spence, S., Burrows, J.F., Elliott, J., Carroll, H.P., Brennan, K., Gabhann, J.N., Coulter, W.A., Johnston, J.A., and Jefferies, C.A. (2009). Siglec-E Is Up-Regulated and Phosphorylated Following Lipopolysaccharide Stimulation in Order to Limit TLR-Driven Cytokine Production. The Journal of Immunology *183*, 7703-7709. 10.4049/jimmunol.0902780.

49. Ciesielska, A., Matyjek, M., and Kwiatkowska, K. (2021). TLR4 and CD14 trafficking and its influence on LPS-induced pro-inflammatory signaling. Cellular and Molecular Life Sciences *78*, 1233-1261. 10.1007/s00018-020-03656-y.

50. Klaus, C., Liao, H., Allendorf, D.H., Brown, G.C., and Neumann, H. (2021). Sialylation acts as a checkpoint for innate immune responses in the central nervous system. Glia *69*, 1619-1636. 10.1002/glia.23945.

51. Holehouse, A.S., and Kragelund, B.B. (2024). The molecular basis for cellular function of intrinsically disordered protein regions. Nature Reviews Molecular Cell Biology *25*, 187-211. 10.1038/s41580-023-00673-0.

52. Silva, Z., Rabaca, J.A., Luz, V., Lourenco, R.A., Salio, M., Oliveira, A.C., Bule, P., Springer, S., and Videira, P.A. (2024). New insights into the immunomodulatory potential of sialic acid on monocyte-derived dendritic cells. Cancer Immunol Immunother *74*, 9. 10.1007/s00262-024-03863-7.

53. Bull, C., Collado-Camps, E., Kers-Rebel, E.D., Heise, T., Sondergaard, J.N., den Brok, M.H., Schulte, B.M., Boltje, T.J., and Adema, G.J. (2017). Metabolic sialic acid blockade lowers the activation threshold of moDCs for TLR stimulation. Immunol Cell Biol *95*, 408-415. 10.1038/icb.2016.105.

54. Miyagi, T., and Yamaguchi, K. (2012). Mammalian sialidases: Physiological and pathological roles in cellular functions. Glycobiology *22*, 880-896. 10.1093/glycob/cws057.
55. Aljohani, M.A., Sasaki, H., and Sun, X.L. (2024). Cellular translocation and secretion of sialidases. J Biol Chem *300*, 107671. 10.1016/j.jbc.2024.107671.
56. Sundararaj, K., Rodgers, J., Angel, P., Wolf, B., and Nowling, T.K. (2021). The role of neuraminidase in TLR4-MAPK signalling and the release of cytokines by lupus serum-stimulated mesangial cells. Immunology *162*, 418-433. 10.1111/imm.13294.
57. Amith, S.R., Jayanth, P., Franchuk, S., Finlay, T., Seyrantepe, V., Beyaert, R., Pshezhetsky, A.V., and Szewczuk, M.R. (2010). Neu1 desialylation of sialyl alpha-2,3-linked beta-galactosyl residues of TOLL-like receptor 4 is essential for receptor activation and cellular signaling. Cell Signal *22*, 314-324. 10.1016/j.cellsig.2009.09.038.
58. Wang, Y., Khan, A., Antonopoulos, A., Bouché, L., Buckley, C.D., Filer, A., Raza, K., Li, K.-P., Tolusso, B., Gremese, E., et al. (2021). Loss of α2-6 sialylation promotes the transformation of synovial fibroblasts into a pro-inflammatory phenotype in arthritis. Nature Communications *12*. 10.1038/s41467-021-22365-z.
59. FlowJo™ Software. Version 10.10.0. Becton, Dickinson and Company (2023).
60. R Development Core Team (2023). A Language and Environment for Statistical Computing (R Foundation for Statistical Computing, Vienna, Austria).
61. Rueden, C.T., Schindelin, J., Hiner, M.C., DeZonia, B.E., Walter, A.E., Arena, E.T., and Eliceiri, K.W. (2017). ImageJ2: ImageJ for the next generation of scientific image data. BMC Bioinformatics *18*, 529. 10.1186/s12859-017-1934-z.
62. Meng, E.C., Goddard, T.D., Pettersen, E.F., Couch, G.S., Pearson, Z.J., Morris, J.H., and Ferrin, T.E. (2023). <scp>UCSF ChimeraX</scp>: Tools for structure building and analysis. Protein Science *32*. 10.1002/pro.4792.
63. R Development Core Team (2023). A Language and Environment for Statistical Computing. R Foundation for Statistical Computing, Vienna, Austria. https://www.R-project.org/.
64. Wickham, H., Hester, J., Bryan, J. (2024). readr: Read Rectangular Text Data. R package version 2.1.5. https://CRAN.R-project.org/package=readr.
65. Wickham, H., Averick, M., Bryan, J., Chang, W., McGowan, L.D.A., François, R., Grolemund, G., Hayes, A., Henry, L., Hester, J., et al. (2019). Welcome to the {tidyverse}. Journal of Open Source Software *4*, 1686. 10.21105/joss.01686.
66. Csárdi, G., . Nepusz, T,. Traag, V,. Horvát, Sz,. Zanini, F,. Noom, D,. Müller, K. (2025). igraph: Network Analysis and Visualization in R. doi.org/10.5281/zenodo.7682609.
67. Pedersen L. T (2024). ggraph: An Implementation of Grammar of Graphics for Graphs and Networks. R package version 2.2.1. https://CRAN.R-project.org/package=ggraph.
68. Wickham, H. (2016). ggplot2: Elegant Graphics for Data Analysis. Springer-Verlag New York.
69. Wickham, H., . Pedersen, T,. Seidel, D. (2023). _scales: Scale Functions for Visualization_. R package version 1.3.0, <https://CRAN.R-project.org/package=scales>.